Results in Chemistry 3 (2021) 100195

Contents lists available at ScienceDirect

Results in Chemistry

journal homepage: www.sciencedirect.com/journal/results-in-chemistry

Potential SARS-CoV-2 3CLpro inhibitors from chromene, flavonoid and hydroxamic acid compound based on FRET assay, docking and pharmacophore studies

Maywan Hariono [a,*], Pandu Hariyono [a], Rini Dwiastuti [a], Wahyuning Setyani [a], Muhammad Yusuf [b], Nurul Salin [c], Habibah Wahab [d]

[a] Faculty of Pharmacy, Sanata Dharma University, Campus III, Paingan, Maguwoharjo, Depok, Sleman 55282, Yogyakarta, Indonesia
[b] Chemistry Department, Faculty of Mathematics and Natural Sciences, Padjadjaran University, Jatinangor, Sumedang 45363, West Java, Indonesia
[c] Malaysian Institute of Pharmaceuticals and Nutraceuticals, National Institute of Biotechnology Malaysia, Halaman Bukit Gambir, 11900 Bayan Lepas, Pulau Pinang, Malaysia
[d] Pharmaceutical Technology Department, School of Pharmaceutical Sciences and USM-RIKEN Centre for Ageing Science (URICAS), Universiti Sains Malaysia, 11800 Minden, Pulau Pinang, Malaysia

ARTICLE INFO

Keywords:
Chromene
Flavonoid
Hydroxamic acid
SARS-CoV-2
3CLpro
In vitro
Docking
Pharmacophore

ABSTRACT

This present study reports some natural products and one hydroxamic acid synthetic compound which were previously reported as matrix metalloproteinase-9 (MMP-9) inhibitors to be evaluated for their inhibition toward severe acute respiratory syndrome coronavirus-2 (SARS-CoV-2) 3-chymotrypsin-like protease (3CLpro). This enzyme is one of the proteins responsible for this coronaviral replication. Two herbal methanolic extracts i.e., *Averrhoa carambola* leaves and *Ageratum conyzoides* aerial part demonstrate >50% inhibition at 1000 μg/mL. Interestingly, apigenin, one of flavonoids, demonstrates 92% inhibition at 250 μg/mL (925 μM) as well as hydroxamic acid compound, *N*-isobutyl-*N*-(4-methoxyphenylsulfonyl)glycyl hydroxamic acid (NNGH), which shows 69% inhibition at 100 μM. The *in vitro* results are supported by the docking studies revealing that the binding mode of both compounds is mainly by interacting with GLU166 residue in the hydrophobic pocket of the 3CLpro. Pharmacophore mapping further supported the results by confirming that the *in vitro* activities of both compounds are due to their pharmacophore features employing hydrogen bond acceptor (HBA), hydrogen bond donor (HBD) and hydrophobic. Gas Chromatography-Mass Spectrometry (GC–MS) analysis reported chromene compounds in *Ageratum conyzoides* aerial part methanolic extract are potential to be this enzyme inhibitor candidate. These all results reflect their potencies to be SARS-CoV-2 inhibitors through 3CLpro inhibition mechanism.

1. Introduction

The global pandemic of severe acute respiratory syndrome-2 (SARS-CoV-2) or coronavirus disease 2019 (Covid-19) has been taking place for at least 1.5 years; giving tremendous impacts in all aspects of life [1]. This becomes worse when neither established vaccines nor antiviral drugs have been found as the treatment against this emergence viral infection [2]. The vaccine produced from many type sources such as viral vector, genetics, inactivated, attenuated, and protein have been implemented to trigger a specific immune response, but the approval is still rolled out to be continued to evolve [3]. A serological-based examination is carried out to measure the antibody level being formed when it is infected by the virus [4]. This has been applied in Covid-19 patients in China and is now commonly referred to as rapid test [5]. Another effort in medical treatment of Covid-19 is by using the blood plasma of the recovered Covid-19 patients [6]. This plasma is expected to contain antibody, to help the Covid-19 patients in critical condition by injection administration. This treatment demonstrates good responses in USA and China due to the ratio of benefit and risk in the patients [7].

Existing drugs being re-purposed for Covid-19 emergence medication are remdesivir (ebola antiviral drug) [8], hydroxychloroquine (antimalaria) [9], ribavirin (RSV antiviral drug) [10], lopinavir and ritonavir (HIV drugs) [11], favipravir and umifenovir (influenza drugs)

* Corresponding author.
E-mail addresses: mhariono@usd.ac.id (M. Hariono), m.yusuf@unpad.ac.id (M. Yusuf), hanim@nibm.my (N. Salin), habibahw@usm.my (H. Wahab).

https://doi.org/10.1016/j.rechem.2021.100195
Received 16 July 2021; Accepted 15 September 2021
Available online 20 September 2021

[12], ivermectin (antiparasite) [13] and camostate mesylate (renal failure drug) [14]. However, as vaccine does, some drugs show either adverse reactions or less clinical benefit which make their use should be strictly controlled [15]. Meanwhile, the discovery of antiviral agent by targeting a diverse protein/ genome demonstrates several potential results to be developed. However, it is still undergoing some more validations [16]. Few compounds have been synthesized in this one year bearing pyrrolidine-dione [17], indole carboxamide [18], phenylpiperidine carboxamide [19], benzothiophene [19] and benzimidazole scaffolds [19], however, they are still in pre-clinical studies.

Instead of synthetic compound being developed, natural products should be one alternative to speed up the discovery of SARS-CoV-2 antiviral agent [20]. Unfortunately, to the best of our knowledge, there has been less studies reporting compounds from natural products having *in vitro/in vivo* activity against the virus. To date, it is 5,6,7-trihydroxy-2-phenyl-4H-chromen-4-one (baicalein), a small molecule from natural resources which has been co-crystallized with 3CLpro of SARS-CoV-2, giving valuable information about the binding mode of this flavonoid into the protease binding site [21].

Other natural compounds reported to combat SARS-CoV are tanshinones, diarylheptanoids and geranylated flavonoids targeting PLpro [22]), quercetine (reverse transcriptase) [23], aloeemodin, and hesperitin (3CLpro) [24], apigenin (viral internal ribosome entry) [25], isatisindigotica (protease) [26], amentoflavone (biflavonoid; protease) [27], glycyrrhizin (protease) [28], tetradrine (viral S and N) [29], silvestrol (cap-dependent viral mRNA translation) [30], etc, which are encouraging to investigate as well against SARS-CoV-2 virus and its protein target. One recent study reports that rocaglates like silvestrol are active against SARS-CoV-2 infected in Vero E6 cells with an EC_{50} of ~ 1.8 nM may be used in first-line antiviral intervention strategies against novel and emerging RNA virus outbreaks [31].

3CLpro is one of proteins responsible for the SARS-CoV-2 life cycle. This enzyme is important in forming the new RNA virus by regulating the viral polypeptide (PP), called PP1a and PP1ab proteolysis. These PPs consist of 11 conserve catalytic cleavage sites, which employ a large hydrophobic pocket containing glutamic acid and other small amino acid residues [32]. This protein is considered as a selective target because to date, there is no known human proteases sharing structural homology and substrate cleavage specificity with SARS-CoV 3CLpro [33].

Our previous study reported some local plants demonstrating significant inhibition toward matrix metalloproteinase-9 (MMP-9), a proteolytic enzyme having roles in extracellular matrix (ECM) degradation which facilitates in-cell migration related to cancer metastasis [34,35]. Since both MMP-9 and 3CLpro are proteolytic enzymes, this prompts us to explore the probability of these plants to be the 3CLpro inhibitor as well. The plants are white frangipani leaves (*Plumeria alba*; IC_{50} 24 μg/mL), goat weed aerial parts (*Ageratum conyzoides*; IC_{50} 64 μg/mL), and star fruit leaves (*Averrhoa carambola*; IC_{50} 77 μg/mL), which were prepared in methanolic extract and tested against MMP-9 using fluorescence resonance energy transfer (FRET)-based assay.

In this present study, we have performed *in vitro* testing for those three plants extracts against SARS-CoV-2 3CLpro enzyme. In addition, we also tested papaya (*Carica papaya*) leaves methanolic extract as this plant had been reported to increase the platelet and leukocyte counts in DENV2-infected AG129 mice associated to the dengue protease inhibition [36]. The most active extract was identified for its existing compounds using gas chromatography-mass spectrometry (GC–MS) and the identified compounds were studied its pharmacophore. Furthermore, we also tested compounds from our laboratory collection including quercetin, apigenin, and *N*-isobutyl-*N*-(4-methoxyphenylsulfonyl)-glycyl hydroxamic acid (NNGH) followed by *in silico* studies using molecular docking and structure-based pharmacophore of the ligands to get the insight mechanism on how they inhibit the SARS-CoV-2 3CLpro activity.

2. Materials and method

2.1. Chemicals

The methanolic extracts of papaya leaves, goat weed aerial parts, white frangipani leaves, and star fruit leaves were courtesy of Drug Discovery Student Club Laboratory, Faculty of Pharmacy, Sanata Dharma University, Indonesia. Apigenin and quercetin were purchased from Sigma Aldrich without further purification, whereas NNGH was purchased from BioVision in the package of MMP-9 inhibitor screening kits. The 3CLpro SARS-CoV-2 kits were purchased from BPS BioSource containing recombinant 3CL-pro SARS-CoV-2 MBP-tag, FRET-based peptide substrate, Tris-HCl buffer, 1,4-Dithiothreitol (DTT) and (2*R*)-1-hydroxy-2-[[(2*S*)-4-methyl-2-(phenylmethoxycarbonylamino)pentanoyl]amino]-3-(2-oxopyrrolidin-3-yl)propane-1-sulfonate sodium (GC376) as the positive control.

2.2. Hardware and software

A laptop with the following specifications: AMD Ryzen 3 2200U, VGA Radeon Vega 3, RAM 4 GB and HDD 1 TB. The 3D protein structure of SARS-CoV-2 3CLpro was collected from protein data bank (PDB 6M2N and 6W63). Other softwares were Marvin Sketch (http://www.chemaxon.com), AutoDockTools1.5.6 package (http://www.autodock.scripps.edu), LigandScout4.4.7 (http://www.inteligand.com) and Biovia Discovery Studio 2020 (http://www.accelrys.com). The ligands (apigenin, quercetin, NNGH, GC376 and all validation sets) were downloaded from PubChem (http://www.pubchem.ncbi.nlm.nih.gov) without further geometrical optimization.

2.3. SARS-CoV-2 3CLpro FRET-based assay

The assay buffer was prepared by adding 12 μL of 0.5 M DTT up to 6 mL of assay buffer which will then be used further. The enzyme and the substrate are separately diluted by adding 3.95 mL and 950 μL of previously prepared assay buffer (with DTT), respectively. The sample for the assay was prepared by dissolving it in DMSO at 100-folds concentration to have the final or required concentration in a 96-well microplate. The final concentration of extracts, apigenin, quercetin, NNGH, GC376, and DMSO were 1000 μg/mL, 250 μg/mL (925 μM), 250 μg/mL (827 μM), 100 μM, 100 μM, and 1%, respectively. Inhibitor control used in this assay called GC376 was diluted in 200 μL of water for injection to have 500 μM solution. Assay was carried by adding solutions in the following order: 30 μL of enzyme (5 ng/μL), required volume of sample or inhibitor (GC376) and assay buffer (with DTT) if necessary up to a total volume of 40 μL. The initial mixture was incubated for 30 min at 25 °C with slow shaking, then followed by the addition of 10 μL of substrate (250 μM) for a mixture with the final volume of 50 μL. The mixtures were then incubated overnight and the fluorescence was measured using Synergy HTX-3 Multi-mode Reader at 360/460 nm [37–39].

2.4. GC–MS analysis

±5 mg of extracts was dissolved in 1 mL of chloroform and then 0.5 μL of them were injected into GC–MS (Shimadzu QP2010 SE). The condition of GC–MS can be described as followed: Rtx 5 MS column (diphenyldiethylpolysiloxane), helium as the mobile phase, 100 °C of column temperature for 5 min and then elevated 5 °C per min until reach 300 °C.

2.5. Molecular docking study

The crystal structures of SARS-CoV-2 3CLpro with their co-crystallized ligands i.e. 5,6,7-trihydroxy-2-phenyl-4H-chromen-4-one (baicalein; PDB 6M2N) [21] and *N*-(4-*tert*-butylphenyl)-*N*-[(1*R*-2-

(cyclohexylamino)-2-oxo-1-(pyridin-3-yl)ethyl]-1H-imidazole-4-carboxamide (X77; PDB 6W63) [40] were individually downloaded from the Protein Data Bank (PDB) (http://www.rcsb.org). The protein PDB 6M2N was presented as a homo-tetramer in the crystal structure. In this study, only one monomer was used; while PDB 6W63 was originally retrieved as a monomer. The ligands were separated from the 3CLpro using Biovia Discovery Studio 2020, saved as a PDB file, and then assigned with Gasteiger Charges using AutoDockTools1.5.6. Both 3CLpros were prepared using the same program in which polar hydrogens were retained and the molecule was assigned by Kollman charges. The grid box was 40, 40, 40 in size with 0.375 Å space and center × = − 9.732, y = 11.403, z = 68.925 for 6M2N, whereas grid box is 30, 30, 30 in size and center × = -19.34, y = 18.376, z = -27.227 were constructed for 6W63. The docking was run 250 times using AutoDock4.2 with default parameters [41]. The control docking (internal validation) was run and defined as valid, when the RMSD values of the complex between the initial and its re-docked poses were less than 2 Å [42]. Upon internal validation, the tested ligands were protonated using Biovia Discovery Studio 2020, given Gasteiger Charge using AutoDockTools1.5.6 and then docked using the parameter used in the control docking against two individual PDBs (6M2N and 6W63). The protein–ligand interactions were visualized using Biovia Discovery Studio 2020.

2.6. Structure-based pharmacophore mapping

The PDB structures were individually uploaded to LigandScout and the pharmacophores were generated using structure-based pharmacophore tool. The external validation was carried out utilising two sets of ligands retrieved from literature [43]. These ligands have been tested against SARS-CoV-2 3CLpro with the same biological condition using *in vitro* FRET-based assay. They show IC_{50} from 1.2 to 468 μM which are defined as active, whereas the ligands having $IC_{50} > 500$ μM are defined as decoy. In this published study, GC376 and quercetin have been identified to have IC_{50} 1.2 μM and > 500 μM, respectively, therefore, in the grouping of validation set, GC376 and quercetin are included in active set and decoy set, respectively. The ligands were screened into the individual pharmacophore using screening tool with the parameters as follow: for PDB 6M2N, scoring functions = pharmacophore-fit; max numbers of omitted features = 2; compounds time out = 0 min; screening mode: match all query features; retrieval mode = stop after first matching conformation; and execution mode = multi-threaded. For 6W63, the parameter is the same, except for the max numbers of omitted features, which was set to 3. The generated receiver operating characteristic (ROC) curve, observed fit-score, and the common pharmacophore features were then analysed [44,45]. Upon validation, the pharmacophore models were used as the filter to identify the testing ligands (apigenin and NNGH) whether they have the pharmacophore features closer to the reference ligands (baicalein and X77). In addition, the pharmacophore of compounds from the most active extract identified by GC–MS were also mapped.

3. Results

The FRET-based assay was used to quantify the SARS-CoV-2 3CLpro activity based on the energy transfer in the fluorogenic peptide substrate, wherein the protease cleaves the peptide link between fluorophore and the peptide moiety. The cleaved fluorophore absorbs the UV energy and then transferred into the peptide moiety while quantifying the energy being emitted [46]. The high fluorescence indicates the high activity of the protease in cleaving the substrate. Therefore, the presence of inhibitor will reduce the protease activity by showing the reduced fluorescence. The positive control used in this experiment is GC376 (see Fig. 1a), a peptidomimetic compound reported to actively inhibit SARS-CoV-2 3CLpro [47]. This compound demonstrates 77% inhibition at 100 μM, indicating the assay system giving true positive response although it is not 100% as stated in the kits brochure. The stability of the SARS-CoV-2 assay kit on shipping could be the reason for the decrease of the positive control. Fig. 1 depicts the four ligands that will be studied as SARS-CoV-2 3CLpro inhibitors.

The extracts were obtained in the same physical and chemical conditions with the previous study conducted [35,36] as it was stored in −20 °C with nitrogen exposure before tightly sealed and its stability was confirmed using thin layer chromatography (TLC). As presented in Fig. 2, three of four plant extracts exhibit inhibitions toward SARS-CoV-2 3CLpro from low to moderate inhibitions. *Carica papaya* inhibits 31% of the protease activity, whereas *Averrhoa carambola* and *Ageratum conyzoides* perform 69% and 83% of inhibition, respectively. Unfortunately, there is no inhibition at all for *Plumeria alba* toward the protease. The negative inhibition could be due to the fluorescence interference of the extract that distracts the fluorescence reading.

Interestingly, apigenin shows 92% inhibition toward the protease; indicating that this is a potential compound to be tested further for SARS-CoV-2 antiviral agent. Quercetin as its analogue shows half

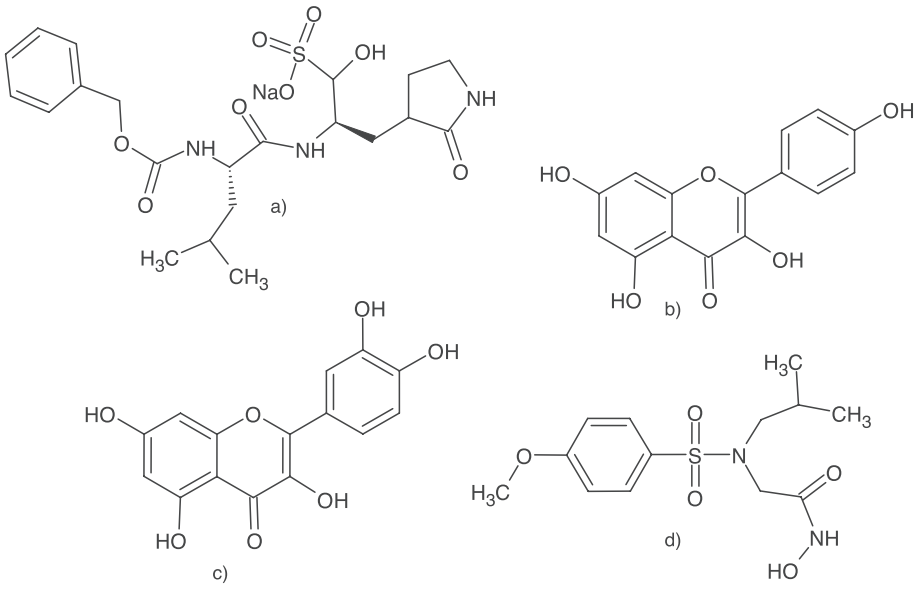

Fig. 1. The structure of a) GC376, b) apigenin, c) quercetin, and d) NNGH.

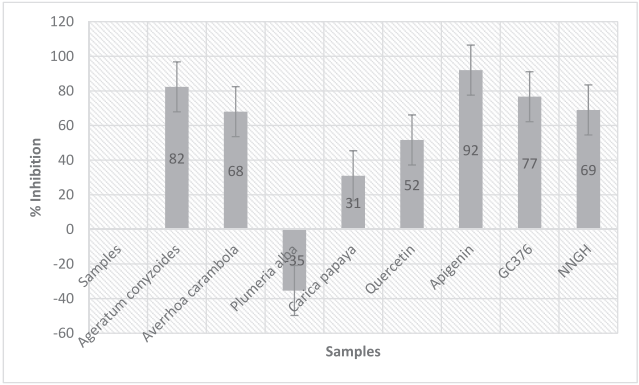

Fig. 2. The inhibition percentage of *Ageratum conyzoides* (1000 μg/mL), *Averrhoa carambola* (1000 μg/mL), *Plumeria alba* (1000 μg/mL), *Carica papaya* (1000 μg/mL), quercetin (827 μM), apigenin (925 μM), GC376 (positive control; 100 μM), and NNGH (100 μM) toward SARS-CoV-2 3CLpro by FRET-based assay.

activity of apigenin (52% inhibition) toward the corresponding enzyme, reflecting the potential of flavonoid class compound to be explored as SARS-CoV-2 antiviral agent. Not so far behind, NNGH as MMP9 inhibitor also displays 69% inhibition toward the protease, indicating the relationship between MMP9 inhibitor with SARS-CoV-2 3CLpro inhibitor.

The potential SARS-CoV-2 3CLpro inhibitor of *Ageratum conyzoides* aerial part methanolic extract encourages us to identify the presence of compounds in this sample using GC–MS. As illustrated in Fig. 3, the GC chromatogram shows eight peaks which are detailed their information in Table 1. They could be classified into three classes of compound employing chromene (peak 1–4), terpene (peak 5 and 6), and fatty acid-like compound (peak 7 and 8). However, GC method is only able to identify compounds which are volatile, therefore, there should be more compounds observed if other general method such as liquid chromatography-mass spectrometry (LC-MS) were applied.

Table 1
The identified compounds from *Ageratum conyzoides* aerial part methanolic extract GC–MS.

Peaks	R_t (minute)	Area (%)	Molecular Weight (g/mol)	Compounds
1	16.190	55.01	220	6,7-dimethoxy-2,2-dimethyl-2H-chromene
2	16.499	6.24	216	6-vinyl-7-methoxy-2,2-dimethylchromene
3	16.872	10.43	216	3,3-dimethyl-7-*tert*-butyl-1-indanone
4	17.149	3.38	248	evodionol
5	18.217	5.25	222	patchouli alcohol
6	19.094	3.91	278	neophytadiene
7	21.944	6.77	270	hexadecenoic acid, methyl ester
8	24.513	8.99	312	octadecanoic acid ester, ethyl ester

Molecular docking study was performed to approach the insight molecular mechanism on how the compounds are able to inhibit the activity of SARS-CoV-2 3CLpro. Therefore, this could give an idea to further optimize the molecule based on the structure activity relationships and then implement it in a rational drug design. The consideration in choosing 6M2N and 6W63 3CLpro as the PDB structures is because on one hand, 6M2N has been co-crystallized with baicalein, a flavonoid compound which is suitable for predicting the binding of new compounds having flavonoid structure such as apigenin and quercetin. On the other hand, 6W63 was selected due to the co-crystallized ligand i.e., X77 having peptide-like structure that is suitable for GC376 as well as NNGH binding prediction. The study was initiated by validating the 3CLpro 3D structure by redocking the co-crystallized ligands to check how similar the docking pose is, between the original and the redocking poses. The result shows that the RMSD value of redocking poses are 0.97 Å and 1.08 Å for PDB 6M2N and PDB 6W63, respectively. This indicates a high similarity between the initial and the redocking pose. Therefore, the 3D structure of 3CLpro along with the docking parameters being

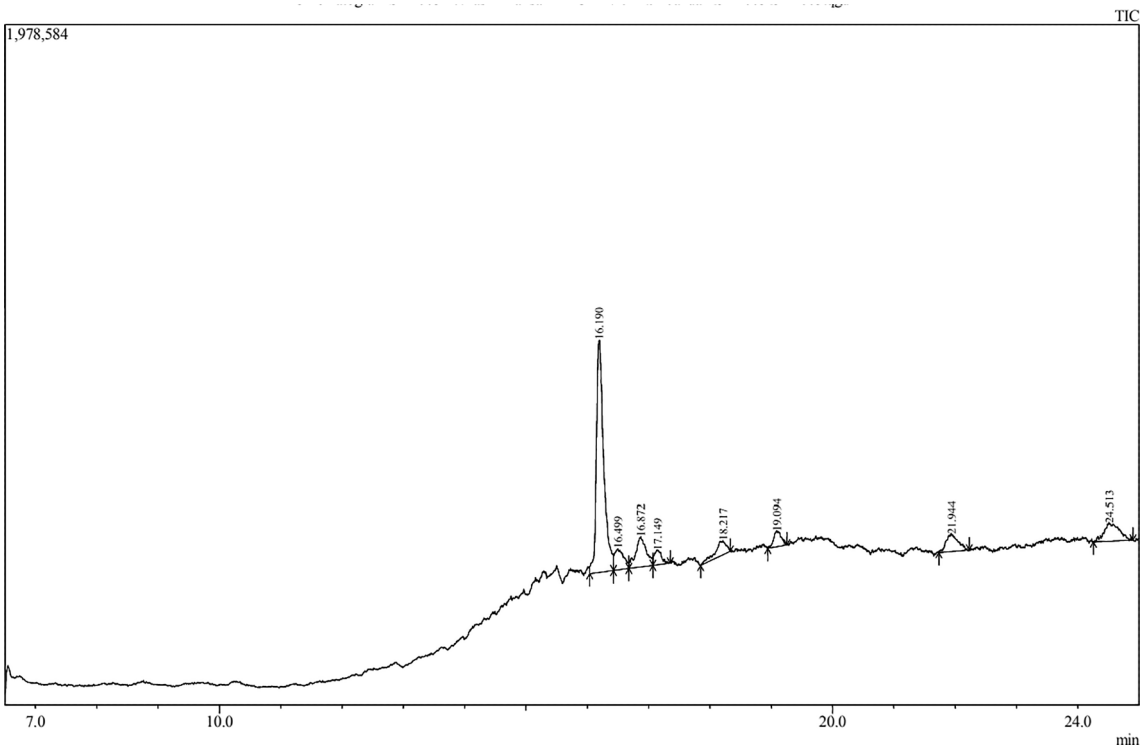

Fig. 3. The GC chromatogram of *Ageratum conyzoides* aerial part methanolic extract shows eight resolved peak at R_t 16.190 to 24.513 min.

used are accepted to be used as the protein model.

Fig. 4 presents the superposition of baicalein and X77 from the control docking over their initial poses in complexed with the 3CLpro. On one hand, baicalein shows ΔG_{bind} of the ligand–protein interaction −6.38 kcal/mol, indicating an acceptable affinity of the ligand toward the 3CLpro. This affinity is contributed by H-bond interaction between baicalein with GLY143 and GLU166. Non-bonding interaction involving hydrophobic characters of either ligand or the protein are also indicated such as the interactions with HIS41, CYS44, MET49, LEU141, and ASN142. On the other hand, X77 demonstrates −9.56 kcal/mol of ΔG_{bind} when interacting with the 3CLpro. This energy is even lower than baicalein; associating a stronger binding with the 3CLpro. However, the binding mode of X77 is highly similar with baicalein, possessing H-bond interactions with GLY143 and GLU166. Two hydrophobic interactions are also notified with ASN142 and MET165.

Furthermore, the accepted docking parameter was applied in the study of molecular interaction between individual quercetin, apigenin, GC376 and NNGH with the 3CLpro. The docking results are presented in Table 2 and the molecular interactions are visualized in Fig. 5 and Fig. 6. Overall, both docking groups (in 6M2N and 6W63) show the same trend in the order of ΔG_{bind} (kcal/mol) from the lowest to the highest energies as follow: GC376 (-9.41; −7.49), apigenin (−6.86; −6.78), quercetin (-6.69; −6.66) and NNGH (-5.56; −5.59). In addition, flavonoids, apigenin and quercetin show comparable energies with baicalein since they are in the same class of flavonoid compound. In contrast, they show quite much higher ΔG_{bind} than X77 in the 3CLpro binding. GC376 always shows the lowest binding energy among others, confirming the true positive data of this peptidomimetic compound. NNGH is a hydroxamic acid MMP inhibitor that shows the highest ΔG_{bind} among others. However, this is still comparable with the flavonoid compounds.

The binding modes of four tested ligands are considered similar despite missing one or more residues for each other's. The most common residues are GLY143 and GLU166, describing the same binding mode of all four tested ligands with the reference ligands (baicalein and X77). Other additional H-bond interactions such as HIS41, CYS44, TYR54, LEU141, ASN142, SER144, HIS163, HIS164, MET165, ASP187, ARG188, GLN189, and GLN192 might contribute to the lower ΔG_{bind} of the four tested ligands compared to baicalein. X77 only has two H-bond interactions but the ΔG_{bind} is much lower than the four tested ligands, describing how effective and selective this reference ligand in binding the 3CLpro enzyme.

In the structure-based pharmacophore, all tested ligands are mapped

Table 2
The docking results of four tested ligands (quercetin, apigenin, GC376, and NNGH) in the active site of SARS-CoV-2 3CLpro using 2 PDB structures (6M2N and 6W63) compares to the reference ligands (baicalein and X77).

Ligands	6M2N		6W63	
	ΔG_{bind} (kcal/mol)	H-Bond interaction	ΔG_{bind} (kcal/mol)	H-Bond interaction
baicalein	−6.38	GLY143, GLU166	na	na
X77	na	na	−9.56	GLY143, GLU166
quercetin	−6.69	HIS41, LEU141, SER144, GLU166	−6.66	GLY143, GLU166, ASN142, HIS163, ARG188, GLN192,
apigenin	−6.86	TYR54, CYS44, HIS41, GLU166, ASP187	−6.78	ASN142, GLY143, GLU166, ARG188
GC376	−9.41	LEU141, ASN142, GLY143, GLU166	−7.49	LEU141, GLY143, HIS164, MET165, GLU166 GLN189
NNGH	−5.56	HIS164, GLU166, GLN192,	−5.59	MET165, GLU166, ARG188

na = not applied.

to the pharmacophore model generated from the individual complex of 3CLpro with their reference ligands i.e., baicalein (6M2N) and X77 (6W63). Baicalein is identified to have seven pharmacophore features employing five hydrogen bond acceptors (HBAs) and two hydrophobic features which are suggested to interact with GLY143, SER144, GLU166, water, THR25, MET49, and GLN189, respectively. These features are generated from two carbonyl oxygens, three hydroxyl oxygens and two benzene rings (see Fig. 7a). The pharmacophore forms a pentagon shape with inter-distances which were measured at 2.38 – 6.33 Å. In PDB 6W63, X77 is generated into four HBAs and two hydrogen bond donors (HBDs) (Fig. 7b). The interacting residues are mainly GLY143 and GLU166 supported with three water molecules. The pharmacophore also forms pentagon shape with inter-distances were measured at 2.18–7.63 Å.

The external validation generated ROC curves for both 6M2N and 6W63 pharmacophore models as presented in Fig. 8. ROC is used to measure a performance of a model which can discrimminate a data either they are true positive, true negative, false positive or false negative [48]. These data are furtherly expressed in an extrapolation of the true positive rate (sensitivity) versus its false positive rate (1-specificity) through the spesific thresholds. A good ROC will generate area under

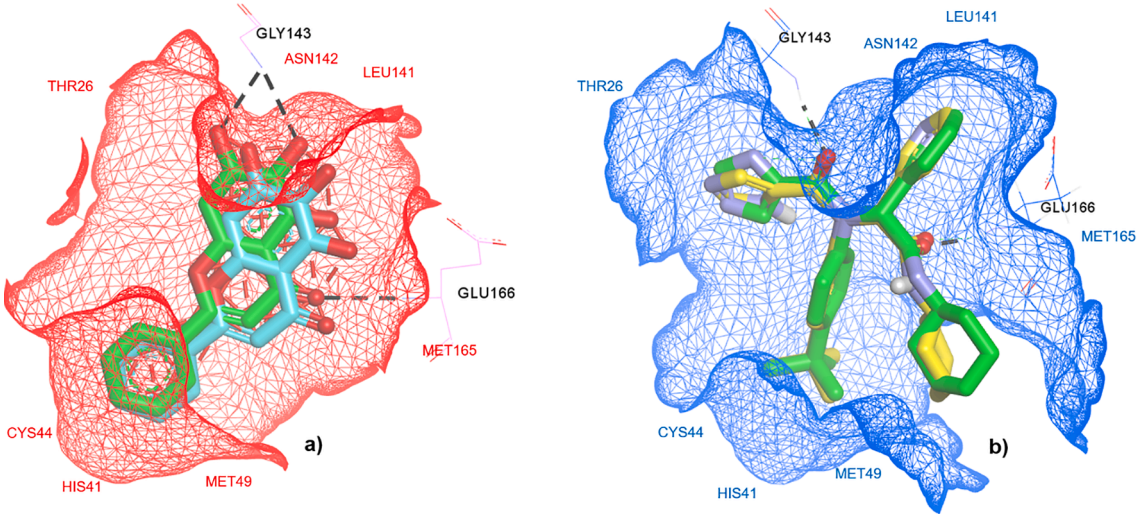

Fig. 4. Overlapping poses of a) baicalein and b) X77 within the active site of 3CLpro SARS-CoV-2. The carbon of the initial pose is green, as for the redocking pose is colored by blue (baicalein) and yellow (X77). (For interpretation of the references to colour in this figure legend, the reader is referred to the web version of this article.)

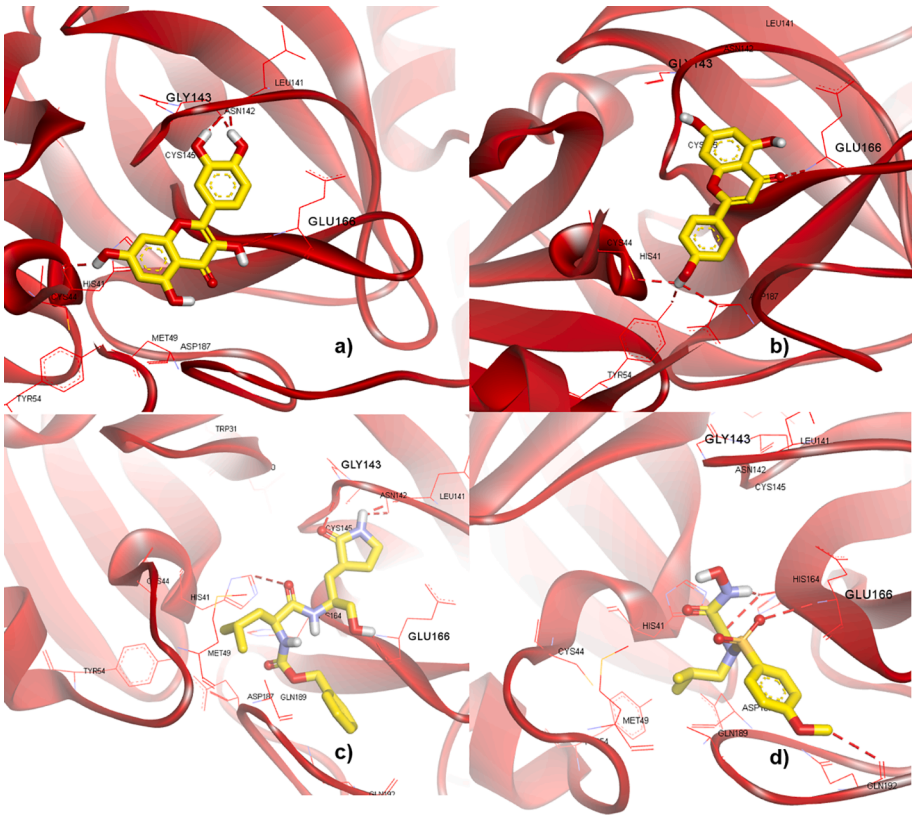

Fig. 5. Molecular interactions of a) quercetin, b) apigenin, c) GC376, and d) NNGH with the active site of 3CLpro using PDB 6M2N. The proteins are presented in a red solid ribbon, whereas the ligands are in stick model colored by yellow (C), white (H), red (O), and blue (N). The H-bond interactions are presented in red dashed lines. (For interpretation of the references to colour in this figure legend, the reader is referred to the web version of this article.)

curve (AUC) up to 100% as well as its enrichmment factor (EF). The 6M2N pharmacophore exhibits AUC in the tresholds 1, 5, 10, and 100% as follows: 1, 1, 1, and 0.7, respectively, whereas the EF in the tresholds 1, 5, 10, and 100% are 0, 3, 2.6 and 1.3, respectively. This AUC is considered good because the value is close to 100% (1). In addition, the EF reflects that in the treshold 1, 5, 10 and 100%, the active compound was found respectively 0, 3, 2.6 and 1.3 times greater than it would be expected. It is not so far behind, the 6W63 pharmacophore shows $AUC_{1, 5, 10, 100}$ are close to 100%, whereas the $EF_{1, 5, 10, 100}$ found active compound 0, 5.9, 2.6, and 1.1 times greater than it would be expected. Overall, based on the AUC and EF, 6M2N has a stronger hypothesis than 6W63.

The 6M2N pharmacophore model succesfully predicts seven true positive compounds of eight would be expected on one hand (see Fig. 9a), and on the other hand, 57 compounds are falsely predicted from 87 decoys would be expected (see Fig. 10a). Furthermore, although the 6W63 pharmacophore model is able to predict the whole active compound as the true positive (see Fig. 9b), however, there are more false negative compound (81 of 87 decoy) found in this model (see Fig. 10b).

The validated pharmacophore is then used as the queries to map the two tested ligands resulting in Pharmacophore Fit-score as follow: apigenin (56.35) and NNGH (57.22). In addition, quercetin (57.35), and GC376 (57.96) were scored in the 6M2N model (see Table 3). Apigenin as well, is able to fit 4 HBAs through its carbonyl O (2 HBAs), phenolic O (2 HBAs), and benzene ring (1 hydrophobic) (Fig. 11a). Those HBA atoms interact with GLU166, water, and SER144, respectively, while the benzene hydrophobically interacts with two residues, i.e., with MET49 and GLN189. NNGH is able to fit pharmacophore through alkoxy O (1 HBA), sulfonyl O (2 HBAs), benzene ring (1 hydrophobic) and isopropyl C (1 hydrophobic) (Fig. 11b) while interacting with respectively, GLY143, GLU166, water, MET49, GLN189, and THR25. GC376 fits to five HBAs through sulfonyl O (1 HBA), hydroxyl O-S (1 HBA), hydroxyl O (1 HBA) and carbonyl O (2 HBAs) (Fig. 11c), with their respective interactions as follow: SER144, GLY143, GLU166 and water. Quercetin is able to fit the pharmacophore model due to the presence of enolic O (2 HBAs), phenolic O (2 HBAs), and benzene (1 hydrophobic) (Fig. 11d). The enolic O interacts with GLU166 and water, while two phenolic O interact with GLY143 and SER144. Furthermore, the benzene well interacts with THR25.

In the external validation using 6W63 pharmacophore model, quercetin was scored as 37.99 and unexpectedly, GC376 was scored as 36.66. This false negative in GC376 reflects the weak hypothesis of 6W63 pharmacophore model as represented by its ROC curve. The pharmacophore fit-score for the two tested ligands are apigenin (38.27) and NNGH (45.07).

Apigenin employs 3 HBAs through carbonyl O (1 HBA with water) and phenolic O (2 HBAs with GLY143 and water, respectively) (Fig. 12a), whereas NNGH fits the pharmacophore through carbonyl O (1 HBA with GLU166), sulfonyl O (2 HBAs with GLY143 and water, respectively), and amine H (1 HBD with water) in Fig. 12b. Furthermore, GC376 fits the pharmacophore through carbonyl O (1 HBA with GLU166), hydroxyl O-S (1 HBA with water), and hydroxyl O (2 HBAs with GLY143 and water, respectively; Fig. 12c), and lastly, quercetin fits to pharmacophore features of X77 through 2 phenolic O (2 HBAs with GLY143 and water), 1 enolic O (with GLU166) and phenolic H (1 HBD) with water (Fig. 12d).

The compounds identified in *Ageratum conyzoides* aerial part methanolic extract are worth to be screened its potency as SARS-CoV-2 3CLpro using structure-based pharmacophore. From this work, it is observed that only two compounds are fit to 6M2N pharmacophore model i.e., 6,7-dimethoxy-2,2-dimethyl-2H-chromene (Fit-score 65.74) and evodionol (Fit-score 65.73). Both compounds show common features employing five HBAs and two hydrophobic (see Fig. 13). 6,7-dimethoxy-2,2-dimethyl-2H-chromene fits to HBAs through its methoxy and

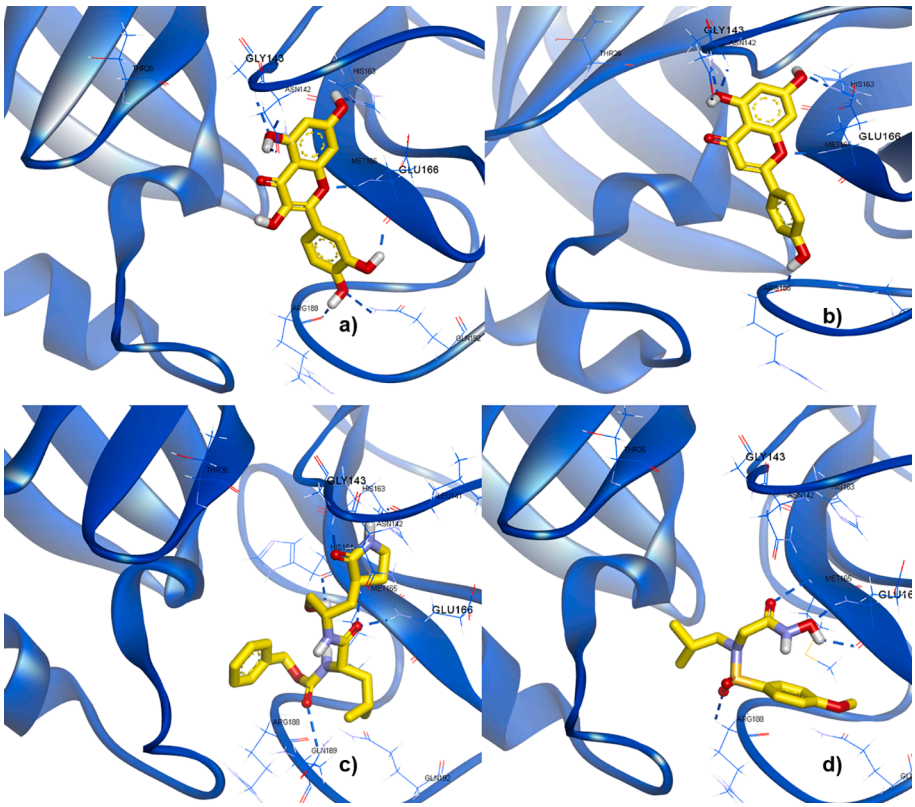

Fig. 6. Molecular interactions of a) quercetin, b) apigenin, c) GC376, and d) NNGH with the active site of 3Clpro using PDB 6W63. The proteins are presented in a blue solid ribbon, whereas the ligands are in stick model colored by yellow (C), white (H), red (O), and blue (N). The H-bond interactions are presented in blue dashed lines. (For interpretation of the references to colour in this figure legend, the reader is referred to the web version of this article.)

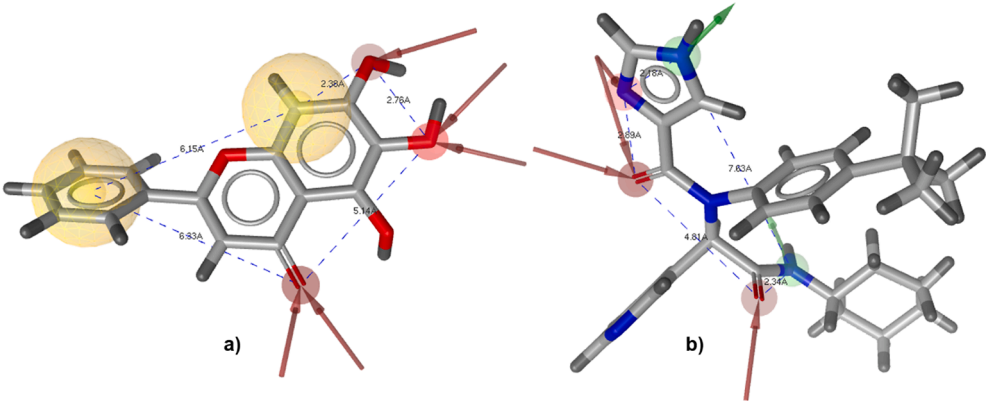

Fig. 7. The pharmacophore features of a) baicalein and b) X77 within the active site of 3CLpro SARS-CoV-2. The ligands are in stick model colored by grey (C), deep grey (H), red (O), and blue (N). The HBA features are presented in red spheres, whereas the HBD and hydrophobic features are in red and yellow spheres, respectively. (For interpretation of the references to colour in this figure legend, the reader is referred to the web version of this article.)

phenolic O, whereas the methyl C and aromatic C fit to hydrophobic feature. Likewise, evodionol displays fitness in HBA through its methoxy, phenolic and carbonyl O, while the hydrophobic features are fit by the same C does in 6,7-dimethoxy-2,2-dimethyl-2H-chromene. The suggested amino acid residues which contact to these corresponding atoms are also similar employing THR25, MET49, GLY143, SER144, GLU166 and GLN189.

4. Discussion

The plant extracts demonstrating inhibition toward SARS-CoV-2 3CLpro are *Ageratum conyzoidez*, *Averrhoa carambola*, and *Carica papaya*. *Ageratum conyzoides* L. is known to contain terpenoid, sterol, flavonoid, chromene, pyrrolizidine alkaloid, coumarin, pyrrolon, and lignan [49]. Other studies also reported that phytoconstituent includes kaempferol, rhamnoside, quercetin, scutellarein, chromene, stigma-7-en-3-ol, sitosterol, stigmasterol, fumaric acid, caffeic acid, saponin, pyrrolidine alkaloid, ageratochromene derivatives, and alkane are deposited in this plant's leaves [50,51]. The abundance of chromene which is observed using GC–MS in the *Ageratum conyzoides* sample could be a key indicator as the compounds responsible to the activity of the methanolic extract toward the protease. Taking into account, a study related to the toxicological extract of the leaves has been carried out in rats by showing LD_{50} extract equals to 600 mg/kg body weight.

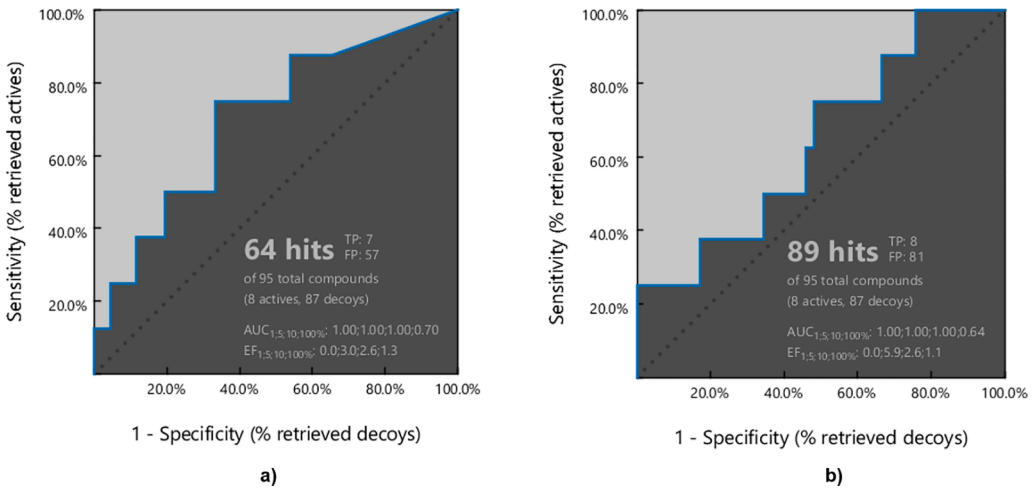

Fig. 8. The ROCs of a) 6M2N and b) 6W63 pharmacophore models.

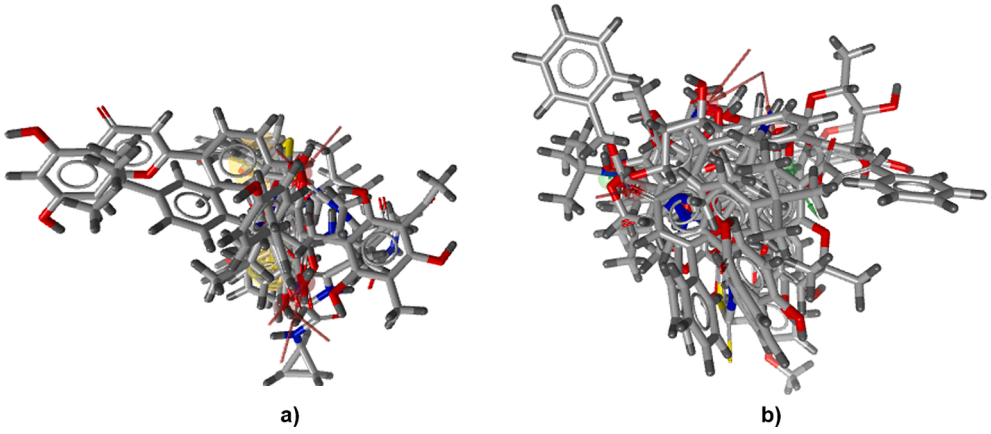

Fig. 9. The overlapping true positive compounds in a) 6M2N and b) 6W63 pharmacophore models.

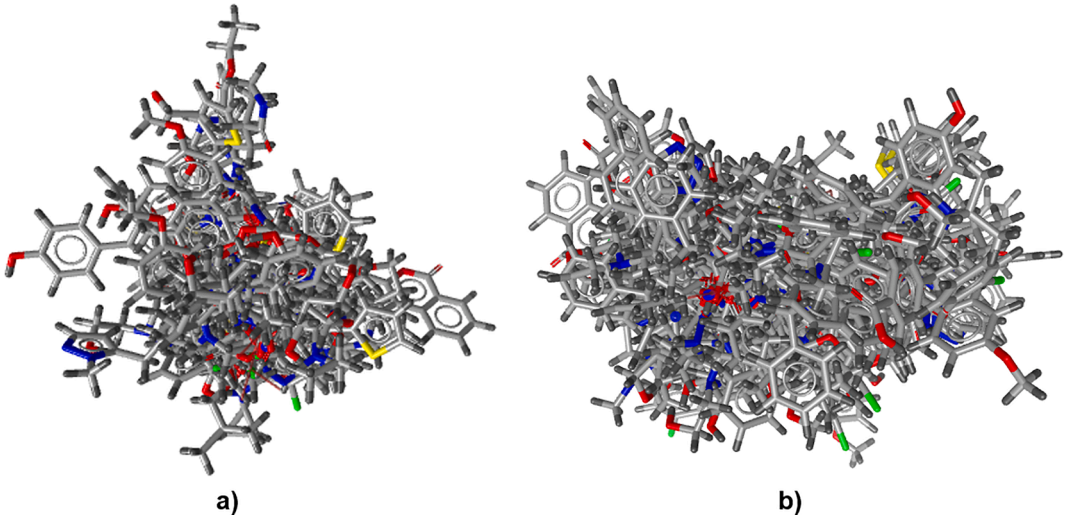

Fig. 10. The overlapping false negative compounds in a) 6M2N and b) 6W63 pharmacophore models.

However, in the chronic toxicity study, the extract did not show a significant effect in the bodyweight elevation, haematology, its alanine amino serum, the aspartate aminotransferase as well as its blood nitrogen urea [52].

In addition, *Averrhoa carambola* leaves are known to contain flavonoid glycoside, such as apigenin- 6-C-*β*-*L*-fucopyranoside and apigenin-6-C-(2″-*O*-α-*L*-rhamnopyranosyl)-*β*-*L* fucopyranoside [53]. Apigenin is detected to have a high inhibition toward the protease, which is in agreement with the knowledge of phytoconstituents, in which apigenin glycosides are contained in the star fruit leaves. In the acute

Table 3
The pharmacophore mapping results of apigenin, NNGH, GC376, and quercetin in the active site of SARS-CoV-2 3CLpro using 2 PDB structures (6M2N and 6W63).

Ligands	6M2N		6W63	
	Fit-score	Matching Features	Fit-score	Matching Features
apigenin	56.35	4 HBA, 1 hydrophobic	38.27	3 HBA
NNGH	57.22	3 HBA, 2 hydrophobic	45.07	3 HBA, 1 HBD
GC376	57.96	5 HBA	36.66	2 HBA, 1 HBD
quercetin	57.35	4 HBA, 1 hydrophobic	37.99	2 HBA, 1 HBD

toxicity assessment, the hydroethanolic extract of *Averrhoa carambola* presented low toxicity in the mice and rats. Furthermore, no signs of toxicity were present in the sub-chronic assessment [54].

Again, flavonoid and its related compound draw an attention to *Carica papaya* albeit lower, which could be responsible toward SARS-CoV-2 3CLpro inhibition. In its particular leaves, there are at least 40 compounds identified in which flavonoid and its analogues present approximately 27%. These flavonoids and its analogues include apigenin, catechin, deoxyquercetin, hesperitin, isorhamnetin, kaempferol, myricetin, naringenin, protocatechuic acid, quercetin, and rutin [37].

The fact that flavonoid is broadly distributed in a high-class plant prompted us to study two of the most common flavonoids in natural products. Flavonoid showed an *in vitro* competitive inhibition in low

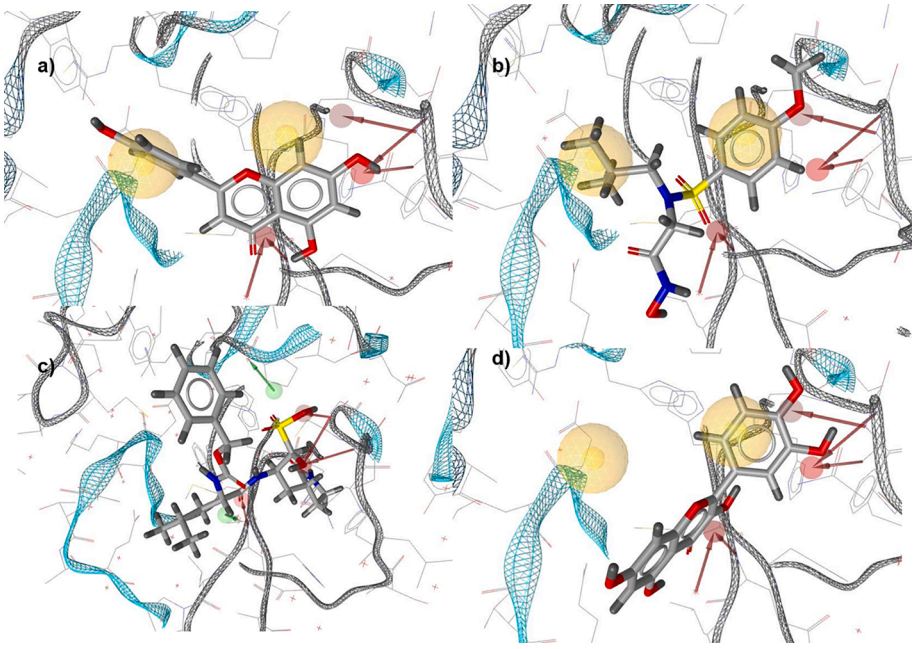

Fig. 11. The pharmacophore features of a) apigenin, b) NNGH, c) GC376, and d) quercetin within the active site of 3CLpro SARS-CoV-2 over the pharmacophore of baicalein (6M2N). The proteins are presented in net ribbon, whereas the ligands are in stick model colored by grey (C), deep grey (H), red (O), blue (N) and yellow (S). The HBA features are presented in red spheres, whereas the hydrophobic features are in yellow spheres. (For interpretation of the references to colour in this figure legend, the reader is referred to the web version of this article.)

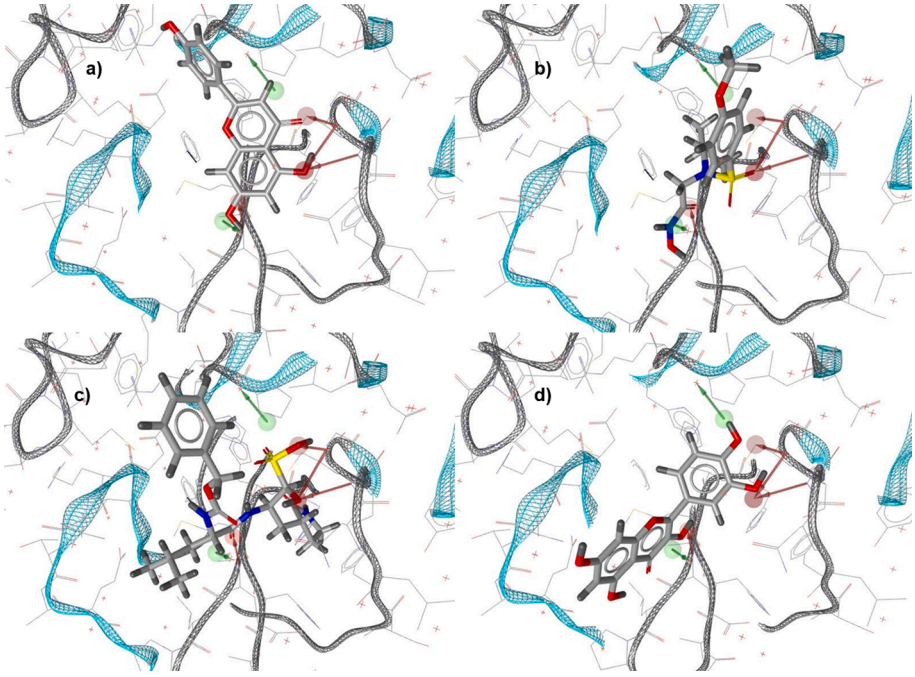

Fig. 12. The pharmacophore features of a) apigenin, b) NNGH, c) GC376, and d) quercetin within the active site of 3CLpro SARS-CoV-2 over the pharmacophore of X77 (6W63). The proteins are presented in net ribbon, whereas the ligand is in stick model colored by grey (C), deep grey (H), red (O), blue (N) and yellow (S). The HBA features are presented in red spheres, whereas the HBD features are in red spheres. (For interpretation of the references to colour in this figure legend, the reader is referred to the web version of this article.)

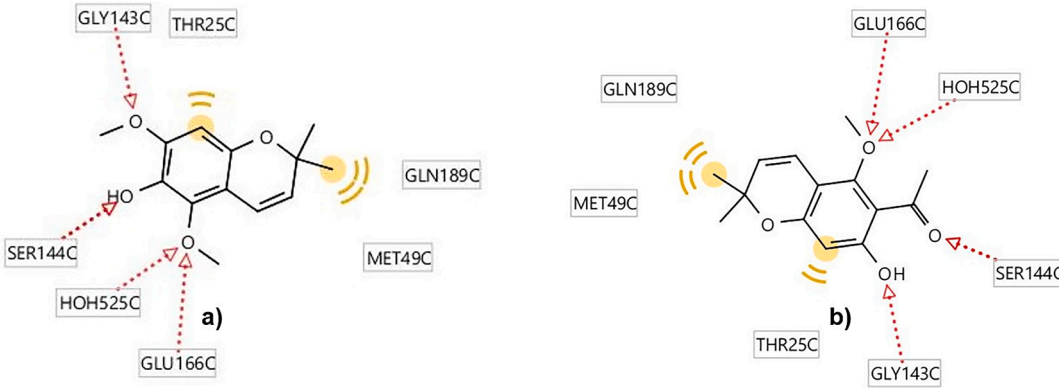

Fig. 13. The 2D visualization of a) 6,7-dimethoxy-2,2-dimethyl-2H-chromene and b) evodionol fit to the pharmacophore model of 6M2N. The red arrow and yellow sphere indicate HBA and hydrophobic features, respectively. (For interpretation of the references to colour in this figure legend, the reader is referred to the web version of this article.)

micromolar activities toward the protease which is in line with the docking explanation. Amentoflavone is the early biflavonoid found active against 3CLpro of SARS-Coronavirus underlining the potency of such compounds to be this protease inhibitor. It was postulated that the presence of benzene ring moiety is at position C-3 of flavones, as biflavone affected 3CLpro inhibitory activity. Amentoflavone is biflavonid, found to inhibit SARS-CoV-2 3CLpro with IC_{50} 143 μM [43]. Compounds bearing more carbonyl groups seem promising to be the protease inhibitor as it is designed to favour a higher nucleophilic attack by serine and cysteine proteases [55,56]. The complex of baicalein with SARS-CoV-2 3CLpro (PDB ID 6M2N) is one of the proofs that flavonoid is such an important feature for 3CLpro pharmacophore.

In this present study, although apigenin and quercetin show>50% inhibition toward the 3CLpro, but their concentrations are still too high to be categorized as active compounds. This actually still needs further study to calculate their IC_{50} to confirm the more representative activity. Unfortunately, due to our limitation, we have not performed this experiment at the moment. However, our present study supported the publication reporting that quercetin competitively inhibited SARS-CoV-2 3CLpro with Ki ~ 7 μM [57], although in another study, quercetin was also reported as inactive compound against SARS-CoV-2 3CLpro [43].

Covalent modifications, redox effects, chelation, autofluorescence, or degradation could be signals leading to the false-positive results under *in vitro* assay condition, which is then called as pan-assay interference compounds (PAINS) [58]. In one published article, apigenin and quercetin had been excluded for further *in silico* testing due to their potencies as PAINS [59], therefore it should be carefully managed in claiming those two flavonoids as active compounds against SARS-CoV-2 3CLpro. However, to the best of our knowledge, there have not been experimentally (by *in vitro*) reported that apigenin and quercetin showed PAINS activities. Therefore, we strongly suggested to conduct this experiment for our future study.

GC376 is a pre-clinical dipeptide-based protease inhibitor, used against feline infectious peritonitis virus (FIPV), a strain of feline coronavirus (FCoV) [60]. Although it is in a low concentration, this peptidomimetic compound has been showing 77% inhibition against SARS-CoV-2 3CLpro. A peptide compound will competitively inhibit the peptide substrate while binding to the 3CLpro active site. Furthermore, although NNGH is a non-peptidic MMP inhibitor [61], but the presence of amide group still associates it with peptide compound, serving as the 3CLpro competitive inhibitor as well. The lower activity of apigenin and quercetin could be due to the fact that they are not peptide-like compound. The pathway on how they perform 3CLpro inhibition could be due to their non-competitive inhibition or via allosteric site. However, further study on x-ray crystallography followed by molecular dynamic simulation is urgently needed.

For further drug development, the cytotoxicity data on a normal cell should be provided. The plumeria and ageratum methanolic extracts have been studied for their cytotoxicity against a normal vero cell using MTT assay in our previous publication [35] showing CC_{50} 225 and 307 μg/ mL, respectively, while the averrhoa methanolic extract had been reported to have non-toxic effect against a normal cell line [62]. On the other hand, papaya methanolic extract have no toxic effect to C6/ 36 cells proliferation by showing CC_{50} 6952 μg/ mL [63]. Apigenin has been reported its safety at high doses in rodent's studies [64], whereas, quercetin as aglycone is marketed as an ingredient of dietary supplements, therefore, it is not cytotoxic [65]. NNGH had been tested its cytotoxicity against NIH/3T3 embryonic cell and showing non-toxic potency [66], while GC376 showed > 150 μM in its CC_{50} against various cell lines reflecting its non-toxic property [67].

In the docking study, GLY143 and GLU166 are two of the common residues indicated in interacting with all ligands. However, in NNGH, the interaction with GLY143 is absent. Interestingly, NNGH keeps showing 69% inhibition in 100 μM of concentration which makes it highly comparable with GC376. This could describe how important GLU166 of the 3CLpro is, to possess polyprotein cleavage during the SARS-CoV-2 replication. The key role of GLU166 could be associated with the essential role of GLU402 in MMP9 which locates this residue in the catalytic centre. In the mechanism of MMP activity, a coordinated bonding between the active site containing Zn^{2+} will chelate the triad of histidine while holding the scissile amide carbonyl of the peptide substrate and water, which is bonded to the GLU402 [68]. The glutamic acid residue stabilizes the water before attacking the carbonyl group of the peptide substrate leading to the proteolysis. The presence of hydroxamic acid group in NNGH will interact with the carboxylate group of GLU residue. Therefore, the proteolysis is inhibited. The same case goes for the SARS-CoV-2 3CLpro. The GLU166 is favourable for NNGH to possess H-bond interaction, which is depicted in the docking results of NNGH in Fig. 5d and 6d. The hydroxamate region is always oriented to the GLU166 to possess the H-bond interactions. In addition, apigenin and quercetin also have hydroxamate-like group i.e., carbonyl and hydroxyl of the chromene ring. In the docking poses (Fig. 5a and b), this region is also oriented to the GLU166. This shows that flavonoid is promising as a competitive inhibitor as well as NNGH and GC376. However, further structural modification is highly needed to reduce the adverse side effect, because hydroxamic acid protease inhibitor is identical with musculoskeletal syndrome.

The recurrent mutation distribution of SARS-CoV-2 mainly occurs in spike (S), nucleocapsid (N), ORF3, ORF8, nsp2, nsp6 and nsp12 proteins. Although it is not as many as the mentioned proteins, the mutation also occurs in 3CLpro (nsp5). T265I (197 viral sequences) is one of the mutations point in 3 chymotrypsin-like proteinase region (3CLpro) [69]. Other literature reported that P108S also occurred in 3 chymotrypsin-like protease (3CLpro) [70] reduces enzymatic activity. To the best of

our knowledge, there has been no report about the mutation in GLU166, therefore, the escape mutation of 3CLpro inhibitor could be still out of concern.

Structure-based pharmacophore mapping is another way to study the ligand–protein binding which concerns the common features like HBA, HBD and hydrophobic in the tested ligand which is mapped to the ligand in complex with the protein active site. The common features in the relative positions (distance) which share high similarity between reference and tested ligand will be fit-scored. Having said that, the model of baicalein (PDB 6M2N), the flavonoids and NNGH share the similar fit-score as well as their common features. The absence of hydrophobic features and the presence of HBD features in the model of X77 (PDB 6W63) definitely change the trend of the fit-score as well as the common features. In this case, 6M2N pharmacophore model with baicalein as the co-crystal ligand demonstrate a more representative hypothesis to predict the activity of SARS-CoV-2 3CLpro inhibitor candidate than 6W63 with X77 as the co-crystal ligand. Furthermore, two chromenes from *Ageratum conyzoides* aerial part methanolic extract, which are actually an integral part of flavonoid scaffold, give insight mechanism on how the extract is capable to inhibit the SARS-CoV-2 3CLpro through the pharmacophore of baicalein (6M2N), leading to a conclusion that this plant is potential for further investigation as SARS-CoV-2 antiviral agent from herbal.

5. Conclusions

A study on four plant extracts employing *Plumeria alba, Carica papaya, Averrhoa carambola* and *Ageratum conyzoides* reveals inactive (−46%), low (31%), moderate (69%) and high (83%) inhibition percentages at 1000 μg/ mL, respectively, toward SARS-CoV-2 3CLpro enzymatic activity. Flavonoid is well distributed among those plants. Due to its chemical structure, it is insightful to be proposed as the 3CLpro inhibitor. This leads us to investigate two flavonoids i.e., apigenin and quercetin to proceed to the *in vitro* study using FRET assay. The results demonstrate that apigenin and quercetin are able to inhibit the 3CLpro activity up to 92% and 52%, respectively, at 250 μg/ mL. The results also support that the plant extracts are potential to be proposed as the herbal remedies in reducing the SARS-CoV-2 viral replication, especially in *Ageratum conyzoides* due to the chromene content. Furthermore, a hydroxamic acid compound, NNGH, also shows 69% inhibition at 100 μM toward SARS-CoV-2 3CLpro, giving more type of the compound's class information as the 3CLpro inhibitor. Computational study using docking and structure-based pharmacophore support the *in vitro* study by describing the insight molecular mechanism on how the chromene, flavonoids and hydroxamic acid possess their activity as the SARS-CoV-2 3CLpro inhibitor candidates.

6. Data availability

The data soft files are available in this below link, and the sample of plant extracts are available upon request. https://drive.google.com/file/d/1T8hzH5540u1hCVl6HMA35j0Dln4Zzhfb/view?usp=sharing

Funding sources

This work was financially supported by Internal Grant of Lembaga Penelitian dan Pengabdian Masyarakat (LPPM), Sanata Dharma University with the grant no. 013/Penel./LPPM-USD/II/2021.

CRediT authorship contribution statement

Maywan Hariono: Conceptualization, Writing - review & editing. **Pandu Hariyono:** Investigation. **Rini Dwiastuti:** Investigation. **Wahyuning Setyani:** Investigation. **Muhammad Yusuf:** Formal analysis, Supervision. **Nurul Salin:** Investigation. **Habibah Wahab:** Conceptualization, Writing - review & editing.

Declaration of Competing Interest

The authors declare that they have no known competing financial interests or personal relationships that could have appeared to influence the work reported in this paper.

Acknowledgement

We greatly acknowledge the Scripps Research Institute, PubChem, ACD/Labs, and Dassault Systems for freely providing AutoDock, 3D structure, ACD/ Chemsketch, and Biovia Discovery Studio softwares.

Appendix A. Supplementary data

Supplementary data to this article can be found online at https://doi.org/10.1016/j.rechem.2021.100195.

References

[1] A. Sharma, S. Tiwari, M.K. Deb, J.L. Marty, Severe acute respiratory syndrome coronavirus-2 (SARS-CoV-2): a global pandemic and treatment strategies, Int. J. Antimicrob. Agents 56 (2) (2020), 106054.
[2] K. Dhama, K. Sharun, R. Tiwari, M. Dadar, Y.S. Malik, K.P. Singh, W. Chaicumpa, COVID-19, an emerging coronavirus infection: advances and prospects in designing and developing vaccines, immunotherapeutics, and therapeutics, Human Vaccines & Immunotherapeutics. 16 (6) (2020) 1232–1238.
[3] S.P. Kaur, V. Gupta, COVID-19 Vaccine: A comprehensive status report, Virus Res. (2020), 198114.
[4] A.H. Mansourabadi, M. Sadeghalvad, H.R. Mohammadi-Motlagh, A. Amirzargar, Serological and Molecular Tests for COVID-19: a recent update, Iranian J. Immunol. 18 (1) (2021) 13–33.
[5] E. Terpos, I. Ntanasis-Stathopoulos, I. Elalamy, E. Kastritis, T.N. Sergentanis, M. Politou, T. Psaltopoulou, G. Gerotziafas, M.A. Dimopoulos, Hematological findings and complications of COVID-19, Am. J. Hematol. 95 (7) (2020 Jul) 834–847.
[6] M. Franchini, G. Marano, C. Velati, I. Pati, S. Pupella, L.G. Maria, Operational protocol for donation of anti-COVID-19 convalescent plasma in Italy, Vox Sang. 116 (1) (2021 Jan) 136–137.
[7] N. Samad, T.E. Sodunke, H. Al Banna, A. Sapkota, A.N. Fatema, K. Iskandar, D. Jahan, T.C. Hardcastle, T. Nusrat, T.S. Chowdhury, M. Haque, Convalescent Plasma Therapy for Management of COVID-19: Perspectives and Deployment in the Current Global Pandemic, Risk Management and Healthcare Policy 13 (2020) 2707.
[8] J.H. Beigel, K.M. Tomashek, L.E. Dodd, A.K. Mehta, B.S. Zingman, A.C. Kalil, E. Hohmann, H.Y. Chu, A. Luetkemeyer, S. Kline, D. Lopez de Castilla, Remdesivir for the treatment of Covid-19, N. Engl. J. Med. 383 (19) (2020 Nov 5) 1813–1826.
[9] A. Qaseem, J. Yost, I. Etxeandia-Ikobaltzeta, M.C. Miller, G.M. Abraham, A. J. Obley, M.A. Forciea, J.A. Jokela, L.L. Humphrey, Should clinicians use chloroquine or hydroxychloroquine alone or in combination with azithromycin for the prophylaxis or treatment of COVID-19? Living practice points from the American College of Physicians (version 1), Ann. Intern. Med. 173 (2) (2020 Jul 21) 137–142.
[10] J.S. Khalili, H. Zhu, N.S. Mak, Y. Yan, Y. Zhu, Novel coronavirus treatment with ribavirin: Groundwork for an evaluation concerning COVID-19, J. Med. Virol. 92 (7) (2020 Jul) 740–746.
[11] C. Schoergenhofer, B. Jilma, T. Stimpfl, M. Karolyi, A. Zoufaly, Pharmacokinetics of lopinavir and ritonavir in patients hospitalized with coronavirus disease 2019 (COVID-19), Ann. Intern. Med. 173 (8) (2020 Oct 20) 670–672.
[12] S.L. Seneviratne, V. Abeysuriya, S. De Mel, I. De Zoysa, R. Niloofa, Favipiravir in COVID-19, International Journal of Progressive Sciences and Technologies. 19 (2) (2020 Apr 19) 143–145.
[13] F. Heidary, R. Gharebaghi, Ivermectin: a systematic review from antiviral effects to COVID-19 complementary regimen, J. Antibiotics. 73 (9) (2020 Sep) 593–602.
[14] P. Breining, A.L. Frølund, J.F. Højen, J.D. Gunst, N.B. Staerke, E. Saedder, M. Cases-Thomas, P. Little, L.P. Nielsen, O.S. Søgaard, M. Kjolby, Camostat mesylate against SARS-CoV-2 and COVID-19—Rationale, dosing and safety, Basic Clin. Pharmacol. Toxicol. 128 (2) (2021 Feb) 204–212.
[15] S.S. Jean, P.R. Hsueh, Old and re-purposed drugs for the treatment of COVID-19, Expert Rev. Anti-infective Therapy. 18 (9) (2020 Sep 1) 843–847.
[16] F. Lamontagne, T. Agoritsas, H. Macdonald, Y.S.J. Leo Diaz, A. Agarwal, J. A. Appiah, Y. Arabi, L. Blumberg, C.S. Calfee, B. Cao, A living WHO guideline on drugs for covid-19, bmj 370 (2020).
[17] D.W. Kneller, G. Phillips, H.M. O'Neill, K. Tan, A. Joachimiak, L. Coates, A. Kovalevsky, Room-temperature X-ray crystallography reveals the oxidation and reactivity of cysteine residues in SARS-CoV-2 3CL Mpro: insights into enzyme mechanism and drug design, IUCrJ 7 (6) (2020).
[18] H. Wang, S. He, W. Deng, Y. Zhang, G. Li, J. Sun, W. Zhao, Y. Guo, Z. Yin, D. Li, L. Shang, Comprehensive insights into the catalytic mechanism of middle east respiratory syndrome 3C-Like protease and severe acute respiratory syndrome 3C-Like protease, ACS Catal. 10 (10) (2020 Apr 28) 5871–5890.

[19] A. Douangamath, D. Fearon, P. Gehrtz, T. Krojer, P. Lukacik, C.D. Owen, E. Resnick, C. Strain-Damerell, A. Aimon, P. Ábrányi-Balogh, J. Brandão-Neto, Crystallographic and electrophilic fragment screening of the SARS-CoV-2 main protease, Nat. Commun. 11 (1) (2020) 1.
[20] M. Omrani, M. Keshavarz, S. Nejad Ebrahimi, M. Mehrabi, L.J. McGaw, M. Ali Abdalla, P. Mehrbod, Potential natural products against respiratory viruses: A perspective to develop anti-COVID-19 medicines, Front. Pharmacol. 11 (2020) 2115.
[21] H.X. Su, S. Yao, W.F. Zhao, M.J. Li, J. Liu, W.J. Shang, H. Xie, C.Q. Ke, H.C. Hu, M. N. Gao, K.Q. Yu, Anti-SARS-CoV-2 activities in vitro of Shuanghuanglian preparations and bioactive ingredients, Acta Pharmacol. Sin. 41 (9) (2020 Sep) 1167–1177.
[22] Y.M. Báez-Santos, S.E. John, A.D. Mesecar, The SARS-coronavirus papain-like protease: structure, function and inhibition by designed antiviral compounds, Antiviral Res. 1 (115) (2015 Mar) 21–38.
[23] R.M. Colunga Biancatelli, M. Berrill, J.D. Catravas, P.E. Marik, Quercetin and vitamin C: an experimental, synergistic therapy for the prevention and treatment of SARS-CoV-2 related disease (COVID-19), Front. Immunol. 19 (11) (2020 Jun) 1451.
[24] K. Chojnacka, A. Witek-Krowiak, D. Skrzypczak, K. Mikula, P. Młynarz, Phytochemicals containing biologically active polyphenols as an effective agent against Covid-19-inducing coronavirus, J. Funct. Foods 30 (2020 Jul), 104146.
[25] R. Jain, S. Shukla, N. Nema, A. Panday, H.S. Gour, A systemic review: structural mechanism of SARS-CoV-2A and promising preventive cure by phytochemicals, Int. J. Immunol. Immunother. 7 (2020) 051.
[26] S.Y. Li, C. Chen, H.Q. Zhang, H.Y. Guo, H. Wang, L. Wang, X. Zhang, S.N. Hua, J. Yu, P.G. Xiao, R.S. Li, Identification of natural compounds with antiviral activities against SARS-associated coronavirus, Antiviral Res. 67 (1) (2005 Jul 1) 18–23.
[27] C.W. Lin, F.J. Tsai, C.H. Tsai, C.C. Lai, L. Wan, T.Y. Ho, C.C. Hsieh, P.D. Chao, Anti-SARS coronavirus 3C-like protease effects of Isatis indigotica root and plant-derived phenolic compounds, Antiviral Res. 68 (1) (2005 Oct 1) 36–42.
[28] J. Cinatl, B. Morgenstern, G. Bauer, P. Chandra, H. Rabenau, H.W. Doerr, Glycyrrhizin, an active component of liquorice roots, and replication of SARS-associated coronavirus, The Lancet. 361 (9374) (2003 Jun 14) 2045–2046.
[29] D.E. Kim, J.S. Min, M.S. Jang, J.Y. Lee, Y.S. Shin, C.M. Park, J.H. Song, H.R. Kim, S. Kim, Y.H. Jin, S. Kwon, Natural bis-benzylisoquinoline alkaloids-tetrandrine, fangchinoline, and cepharanthine, inhibit human coronavirus OC43 infection of MRC-5 human lung cells, Biomolecules. 9 (11) (2019 Nov) 696.
[30] C. Müller, F.W. Schulte, K. Lange-Grünweller, W. Obermann, R. Madhugiri, S. Pleschka, J. Ziebuhr, R.K. Hartmann, A. Grünweller, Broad-spectrum antiviral activity of the eIF4A inhibitor silvestrol against corona-and picornaviruses, Antiviral Res. 1 (150) (2018 Feb) 123–129.
[31] C. Müller, W. Obermann, N. Karl, H.G. Wendel, G. Taroncher-Oldenburg, S. Pleschka, R.K. Hartmann, A. Grünweller, J. Ziebuhr, The rocaglate CR-31-B (−) inhibits SARS-CoV-2 replication at non-cytotoxic, low nanomolar concentrations in vitro and ex vivo, Antiviral Res. 1 (186) (2021 Feb), 105012.
[32] R. Arya, S. Kumari, B. Pandey, H. Mistry, S.C. Bihani, A. Das, V. Prashar, G. D. Gupta, L. Panicker, M. Kumar, Structural insights into SARS-CoV-2 proteins, J. Mol. Biol. 433 (2) (2021 Jan 22), 166725.
[33] S. Ullrich, C. Nitsche, The SARS-CoV-2 main protease as drug target, Bioorg. Med. Chem. Lett. (2020), 127377.
[34] M. Hariono, R. Rollando, I. Yoga, A. Harjono, A. Suryodanindro, M. Yanuar, T. Gonzaga, Z. Parabang, P. Hariyono, R. Febriansah, A. Hermawansyah, Bioguided Fractionation of Local Plants against Matrix Metalloproteinase9 and Its Cytotoxicity against Breast Cancer Cell Models: In Silico and In Vitro Study (Part II), Molecules 26 (5) (2021) 1464.
[35] M. Hariono, R. Rollando, J. Karamoy, P. Hariyono, M. Atmono, M. Djohan, W. Wiwy, R. Nuwarda, C. Kurniawan, N. Salin, H. Wahab, Bioguided Fractionation of Local Plants against Matrix Metalloproteinase9 and Its Cytotoxicity against Breast Cancer Cell Models: In Silico and In Vitro Study, Molecules 25 (20) (2020) 4691.
[36] P. Hariyono, C. Patramurti, D.S. Candrasari, M. Hariono, An integrated virtual screening of compounds from Carica papaya leaves against multiple protein targets of SARS-Coronavirus-2, Results in Chemistry. 3 (2021 Jan), 100113.
[37] J.S. Morse, T. Lalonde, S. Xu, W.R. Liu, Learning from the past: possible urgent prevention and treatment options for severe acute respiratory infections caused by 2019-nCoV, ChemBioChem 21 (5) (2020 Mar 2) 730–738.
[38] L. Zhang, D. Lin, X. Sun, U. Curth, C. Drosten, L. Sauerhering, S. Becker, K. Rox, R. Hilgenfeld, Crystal structure of SARS-CoV-2 main protease provides a basis for design of improved α-ketoamide inhibitors, Science 368 (6489) (2020 Apr 24) 409–412.
[39] M.S. Zubair, S. Maulana, A. Widodo, R. Pitopang, M. Arba, M. Hariono, GC-MS, LC-MS/MS, Docking and molecular dynamics approaches to identify potential SARS-CoV-2 3-chymotrypsin-like protease inhibitors from Zingiber officinale Roscoe, Molecules 28 (26) (2021 August) 5230.
[40] Mesecar AD. A taxonomically-driven approach to development of potent, broad-spectrum inhibitors of coronavirus main protease including SARS-CoV-2 (COVID-19), http://www.rcsb.org/structure/6W63; 2020 (accessed 24 October 20).
[41] G.M. Morris, R. Huey, W. Lindstrom, M.F. Sanner, R.K. Belew, D.S. Goodsell, A. J. Olson, AutoDock4 and AutoDockTools4: Automated docking with selective receptor flexibility, J. Comput. Chem. 30 (16) (2009) 2785–2791.
[42] S.J. De Vries, M. Van Dijk, A.M. Bonvin, The HADDOCK web server for data-driven biomolecular docking, Nat. Protoc. 5 (5) (2010 May) 883.
[43] E. Glaab, G.B. Manoharan, D. Abankwa, A pharmacophore model for SARS-CoV-2 3CLpro small molecule inhibitors and in vitro experimental validation of computationally screened inhibitors, J. Chem. Inf. Model. 61 (8) (2021 Jan 1) 4082–4096.
[44] G. Wolber, T. Langer, LigandScout: 3-D pharmacophores derived from protein-bound ligands and their use as virtual screening filters, J. Chem. Inf. Model. 45 (1) (2005) 160–169.
[45] R. Mardianingrum, M. Yusuf, M. Hariono, A. Mohd Gazzali, M. Muchtaridi, α-Mangostin and its derivatives against estrogen receptor alpha, J. Biomol. Struct. Dyn. 5 (2020 Nov) 1–4.
[46] H.C. Ishikawa-Ankerhold, R. Ankerhold, G.P. Drummen, Advanced fluorescence microscopy techniques—Frap, Flip, Flap, Fret and flim. Molecules. 17 (4) (2012) 4047–4132.
[47] L. Fu, F. Ye, Y. Feng, F. Yu, Q. Wang, Y. Wu, C. Zhao, H. Sun, B. Huang, P. Niu, H. Song, Both Boceprevir and GC376 efficaciously inhibit SARS-CoV-2 by targeting its main protease, Nat. Commun. 11 (1) (2020 Sep 4) 1–8.
[48] M.S. Pepe, Receiver operating characteristic methodology, J. Am. Stat. Assoc. 95 (449) (2000 Mar 1) 308–311.
[49] R. Kaur, N.K. Dogra, A review on traditional uses, chemical constituents and pharmacology of Ageratum conyzoides L. (Asteraceae), Int J Phaemaceutical Biol Arch. 5 (5) (2014) 33–45.
[50] N. Yadav, S.A. Ganie, B. Singh, A.K. Chhillar, S.S. Yadav, Phytochemical constituents and ethnopharmacological properties of Ageratum conyzoides L, Phytother. Res. 33 (9) (2019 Sep) 2163–2178.
[51] J.C. Kotta, A. Lestari, D.S. Candrasari, M. Hariono, Medicinal Effect, In Silico Bioactivity Prediction, and Pharmaceutical Formulation of Ageratum conyzoides L.: A Review, Scientifica. (2020). Oct 13;2020.
[52] B.M. Agaie, P. Nwatsok, M.L. Sonfada, "Toxicological Effect of the Water Extract of Ageratum Conyzoides in Rats," 2000.
[53] D.A. Cabrini, H.H. Moresco, P. Imazu, C.D. Silva, E.F. Pietrovski, D.A. Mendes, A. D. Prudente, M.G. Pizzolatti, I.M. Brighente, M.F. Otuki, Analysis of the potential topical anti-inflammatory activity of Averrhoa carambola L. in mice, Evidence-based Complementary and Alternative Medicine. 2011 (2011).
[54] D.L. Pessoa, M.S. Cartágenes, S.M. Freire, M.O. Borges, A.C. Borges, Acute and sub-chronic pre-clinical toxicological study of Averrhoa carambola L. (Oxalidaceae), Afr. J. Biotechnol. 12 (40) (2013).
[55] Y.B. Ryu, H.J. Jeong, J.H. Kim, Y.M. Kim, J.Y. Park, D. Kim, T.T. Naguyen, S. J. Park, J.S. Chang, K.H. Park, M.C. Rho, Biflavonoids from Torreya nucifera displaying SARS-CoV 3CLpro inhibition, Bioorg. Med. Chem. 18 (22) (2010 Nov 15) 7940–7947.
[56] Y. Hartini, B. Saputra, B. Wahono, Z. Auw, F. Indayani, L. Adelya, G. Namba, M. Hariono, Biflavonoid as potential 3-chymotrypsin-like protease (3CLpro) inhibitor of SARS-Coronavirus, Results in Chemistry. 3 (2021), 100087.
[57] O. Abian, D. Ortega-Alarcon, A. Jimenez-Alesanco, L. Ceballos-Laita, S. Vega, H. T. Reyburn, B. Rizzuti, A. Velazquez-Campoy, Structural stability of SARS-CoV-2 3CLpro and identification of quercetin as an inhibitor by experimental screening, Int. J. Biol. Macromol. 164 (2020 Dec) 1693–1703.
[58] S. Jasial, Y. Hu, J. Bajorath, How frequently are pan-assay interference compounds active? Large-scale analysis of screening data reveals diverse activity profiles, low global hit frequency, and many consistently inactive compounds, J. Med. Chem. 60 (9) (2017 May 11) 3879–3886.
[59] G. Jiménez-Avalos, A.P. Vargas-Ruiz, N.E. Delgado-Pease, G.E. Olivos-Ramirez, P. Sheen, M. Fernández-Díaz, M. Quiliano, M. Zimic, Comprehensive virtual screening of 4.8 k flavonoids reveals novel insights into allosteric inhibition of SARS-CoV-2 MPRO, Sci. Rep. 11 (1) (2021 Jul 29) 1–9.
[60] K. Sharun, R. Tiwari, K. Dhama, Protease inhibitor GC376 for COVID-19: Lessons learned from feline infectious peritonitis, Ann. Medi. Surgery. 61 (2021 Jan) 122–125.
[61] Y. Arendt, L. Banci, I. Bertini, F. Cantini, R. Cozzi, R. Del Conte, L. Gonnelli, Catalytic domain of MMP20 (Enamelysin)–The NMR structure of a new matrix metalloproteinase, FEBS Lett. 581 (24) (2007 Oct 2) 4723–4726.
[62] A.M. Saghir, S, A. Sadikun, F.S. Al-Suede, M.S.A. Majid A, V. Murugaiyah, Antihyperlipidemic, antioxidant and cytotoxic activities of methanolic and aqueous extracts of different parts of star fruit, Curr. Pharm. Biotechnol. 17 (10) (2016 Aug 1) 915–925.
[63] F. Husin, H. Ya'akob, S.N. Abd Rashid, S. Shahar, H.H. Soib, Cytotoxicity study and antioxidant activity of crude extracts and SPE fractions from Carica papaya leaves, Biocatalysis and Agricultural Biotechnology. 19 (2019 May), 101130.
[64] M. Venigalla, S. Sonego, E. Gyengesi, M.J. Sharman, G. Münch, Novel promising therapeutics against chronic neuroinflammation and neurodegeneration in Alzheimer's disease, Neurochem. Int. 95 (2016 May) 63–74.
[65] S. Andres, S. Pevny, R. Ziegenhagen, N. Bakhiya, B. Schäfer, K.I. Hirsch-Ernst, A. Lampen, Safety aspects of the use of quercetin as a dietary supplement, Mol. Nutr. Food Res. 62 (1) (2018) 1700447.
[66] H. Laronha, I. Carpinteiro, J. Portugal, A. Azul, M. Polido, K.T. Petrova, M. Salema-Oom, I. Barahona, J. Caldeira, Polymerizable matrix metalloproteinases' inhibitors with potential application for dental restorations, Biomedicines. 9 (4) (2021 Apr) 366.
[67] Y. Kim, H. Liu, A.C. Galasiti Kankanamalage, S. Weerasekara, D.H. Hua, W. C. Groutas, K.O. Chang, N.C. Pedersen, Reversal of the progression of fatal coronavirus infection in cats by a broad-spectrum coronavirus protease inhibitor, PLoS Pathog. 12 (3) (2016 Mar 30), e1005531.

[68] M. Hariono, S.H. Yuliani, E.P. Istyastono, F.D. Riswanto, C.F. Adhipandito, Matrix metalloproteinase 9 (MMP9) in wound healing of diabetic foot ulcer: Molecular target and structure-based drug design, Wound Medicine. 22 (2018 Sep) 1–3.
[69] O.E. Omotoso, A.D. Babalola, A. Matareek, Mutational hotspots and conserved domains of SARS-CoV-2 genome in African population, Beni-Suef University journal of basic and applied sciences. 10 (1) (2021) 1–7.
[70] K. Abe, Y. Kabe, S. Uchiyama, Y. Iwasaki, H. Ishizu, Y. Uwamino, T. Takenouchi, S. Uno, M. Ishii, M. Takahiro, N. Masanori, Pro108Ser mutant of SARS-CoV-2 3CLpro reduces the enzymatic activity and ameliorates COVID-19 severity in Japan. medRxiv. 2021 Jan 1:2020-11.